Al-Azhar Bulletin of Science

Volume 32 | Issue 2 Article 14

12-31-2021
Section: Earth science

Lineaments Detection and Groundwater Exploration Using GIS and Geo-electric Data at Wadi El-Asyuti Area, Eastern Desert, Egypt.

Ashraf Abdo
Geology Department, Faculty of Science, Al-Azhar University, Cairo, Egypt., geo.ashraf.moh@gmail.com

Hassan Sabet
Geology Department, Faculty of Science, Al-Azhar University, Cairo, Egypt., hassansaleh@yahoo.com

Mohamed Mebed
Geophysics Management, Egyptian Mineral Resources Authority, Egypt., saied2410@yahoo.com

How to Cite This Article

Abdo, Ashraf; Sabet, Hassan; and Mebed, Mohamed (2021) "Lineaments Detection and Groundwater Exploration Using GIS and Geo-electric Data at Wadi El-Asyuti Area, Eastern Desert, Egypt.," *Al-Azhar Bulletin of Science*: Vol. 32: Iss. 2, Article 14.
DOI: https://doi.org/10.21608/absb.2021.84781.1125

Al-Azhar Bulletin of Science, Section D, Vol. 32, No. 2, (December) 2021, pp. 49-59
http://doi.10.21608/absb.2021.84781.1125

Al-Azhar Bulletin of Science: Section D

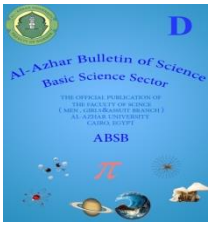

LINEAMENTS DETECTION AND GROUNDWATER EXPLORATION USING GIS AND GEO-ELECTRIC DATA AT WADI EL-ASYUTI AREA, EASTERN DESERT, EGYPT.

Ashraf M. Abdo [a,*], Hassan S. Sabet [a], Mohamed E. Mebed [b]

[a] Geology Department, Faculty of Science, Al-Azhar University, Cairo, Egypt.

[b] Geophysics Management, Egyptian Mineral Resources Authority, Egypt.
*Corresponding Author: geo.ashraf.moh@gmail.com
Received: 21 Jul 2021; Revised: 24 Dec 2021; Accepted: 25 Dec 2021; Published: 31 Dec 2021

ABSTRACT

Geo-electric and GIS data to Wadi El-Asyuti area, central Eastern Desert, Egypt have been used for identify the different lineaments and possibilities of the occurrence of the groundwater. Shaded relief maps were developed from the digital elevation model (DEM) which used for identifying the lineaments. Geomatica software extracted the lineaments at the final maps with NW-SE direction. Meanwhile the geologic fault trends derived from geologic map take NW-SE, WNW-ESE, N-S and ENE-WSW directions. Twenty two electric resistivity soundings were conducted in the study area and three cross sections. Drilled well is near from VES-22. Geo-electric and drilling results reflected three layers. The first one consists of Wadi deposit, friable sand, fine sand, clay and limestone. The second layer composed of clay intercalation with limestone and silt and the third layer consists of clay intercalation with sand and silt and represented the aquifer layer.

Keywords: Wadi El-Asyuti area; Digital elevation model (DEM); Electric resistivity soundings; Groundwater

1. INTRODUCTION

The area under investigation is located at Wadi El Asyuti area, Central Eastern Desert, Egypt. It covers an area about 675.1 km^2 and lies between longitudes 31° 15′ 00″ E and 31° 30′ 00″ E and latitudes 27° 05′ 00″ N and 27° 20′ 00″ N (Fig.1). Wadi El Asyuti area was intensively investigated by many workers [1-6]. The main intent of this study to describe the different lineaments of the study area, identify the subsurface stratigraphic succession of the area and to identify the possibilities of the occurrence of the groundwater in the study area.

2. GEOLOGICAL SETTING

Stratigraphy and surface geological structure of the study area [7]. Figures 2 and 3 shows the different rock units and structural trends in the study area. The litho-stratigraphy of the study area could be divided from the base to the top as the follow; 1) Lower Eocene Rocks which consists of Thebes group (chalky limestone) and Minia Formation (marine limestone). 2) Pliocene deposits are represented by fluviatile siltstone, sandstone and claystone (Issawiya Formation). 3) Quaternary deposits; are represented by prenile, neonile and wadi deposits, fanglomerate and Nile silt. Structurally, there are several faults affecting the area such as the NW-SE related to the Gulf of Suez trend, the Najd fault [8] system trend (WNW-ESE), the N-S trend is related to the East African trend and ENE-WSW correlated with Syrian arc system trend.

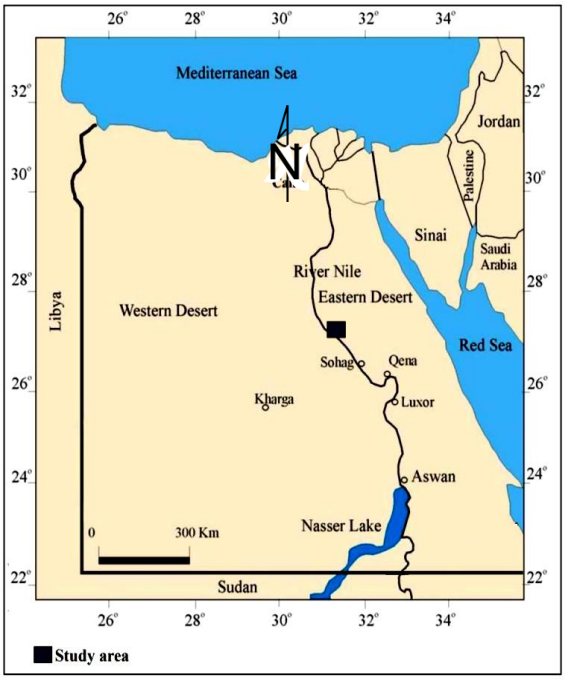

Fig. 1. Location map of the study area.

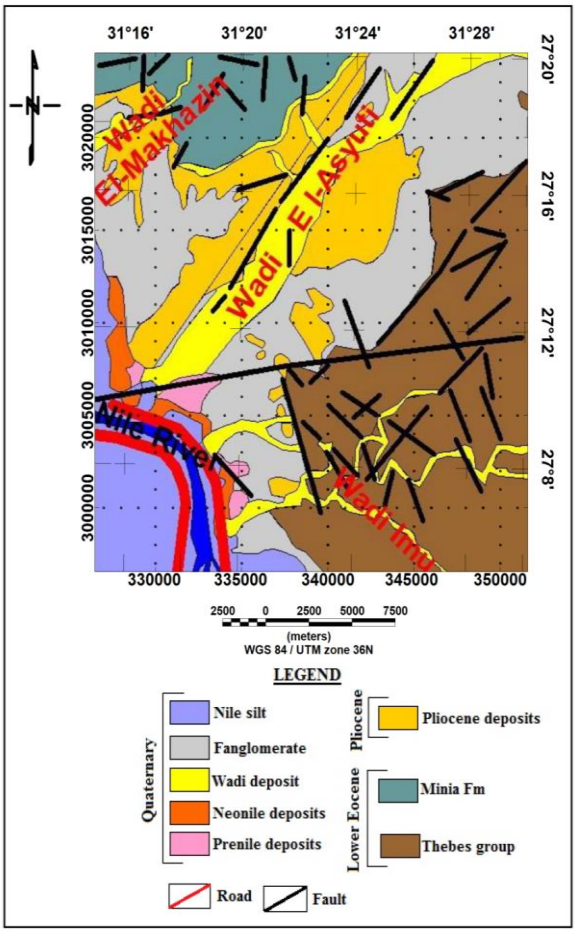

Fig. 2. Detailed geologic map of the study area [7].

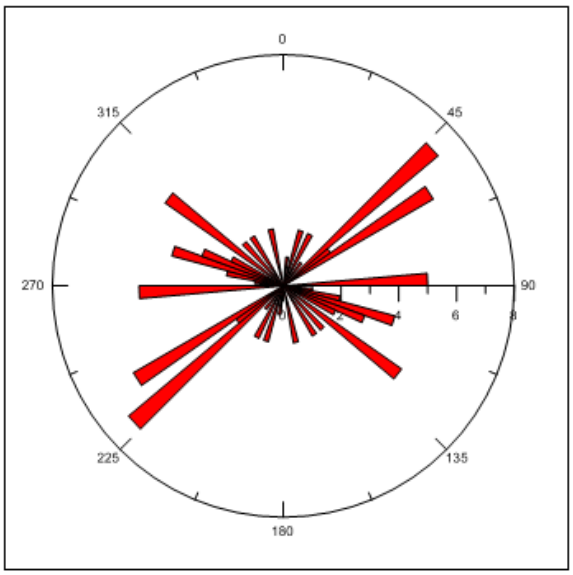

Fig. 3. Rose diagram of the geologic lineaments of the study area.

3. METHODOLOGY AND DATA ACQUISITIONS

3.1. Digital Elevation Model (DEM)

Satellite remote sensing images and SRTM DEM of the area under investigation [9]. The topographic elevation of the study area was represented as shown in Digital elevation model (Fig. 4). The highest elevation located at the eastern parts of the area, while the lowest elevation located at the southwestern parts of the study area.

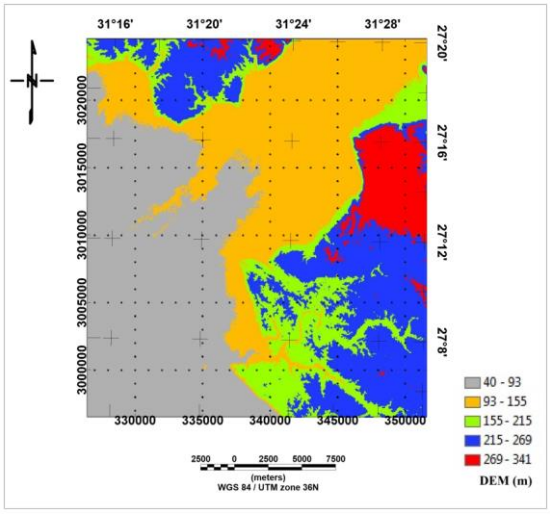

Fig. 4. Digital Elevation Model (DEM) of the study area [9]

3.2. Vertical Electrical Sounding (VES) and drilling data

In the present study, vertical electrical resistivity surveys (VES) using Schlumberger array. Twenty two electric resistivity soundings were conducted in the study area and three cross sections as shown in (Fig. 5). The spacing between the VES's location are controlled by the topographical and geological condition of the site. Field equipment's includes; ELREC-T, IRIS Instruments, dry batteries, iron steel electrodes and wires used to conduct the geo-electrical resistivity surveys in the study area. WELL-1 is near from VES-22. Coordinates of WELL-1 are (longitude; 31° 20.7′ E and latitude; 27° 09.4′ N).

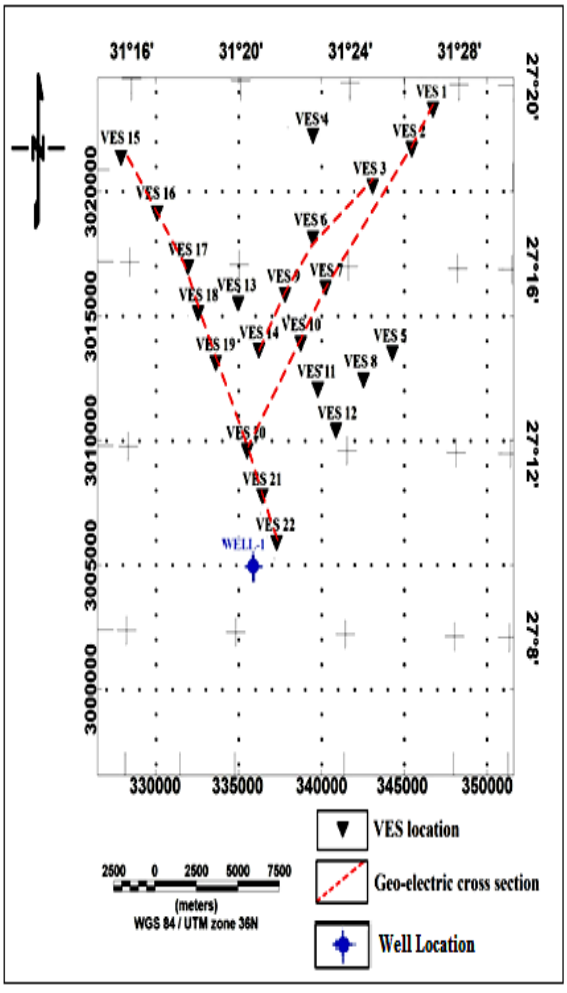

Fig. 5. Location map of VES's, geo-electric cross sections and WELL-1.

4. DATA INTERPRETATION

4.1. Automatic lineaments from shaded DEMs

In order to identify linear topographic features from the DEM, eight shaded relief images were generated. The first step was the production of eight separate shaded relief images with light sources coming from eight different directions. The first created shaded relief image had a solar azimuth (sun angle) of 0°. The other seven shaded relief images were created with seven contrasting illumination directions 45°, 90°,135°, 180°, 225°, 270° and 315° (Figs. 6 a, b, c, d, e, f, g and h).

a) Combine images and lineaments extraction

The second step is to combine four shaded relief images to produce one shaded relief image. For this purpose, the combinations of the four shaded relief maps are computed by using GIS data overlay technique, where the first four shaded relief images are overlaid to produce one image with multi - illumination directions (0°, 45°, 90° and 135°) and the second overlay is to produce one image with multi - illumination directions (180°, 225°, 270° and 315°). By using Geomatica 10.3 software; combine images have been used for automatic lineaments extraction over the study area (Figs. 7 a and b).

b) Rose diagrams of the extracted lineaments

The main trends of the extracted lineaments of both images (combining four shaded relief images with sun angles of 0°, 45°, 90° and 135° and the four shaded relief images with sun angles of 180°, 225°, 270° and 315°) were found to be NW-SE (Figs. 8 a and b).

4.2 Selections of VES's locations using geologic map and DEM

Figures 9 and 10 reflected that; VES's locations located at suitable locations which characterized by; low elevations and locations of accumulate of torrent water and rainfall water.

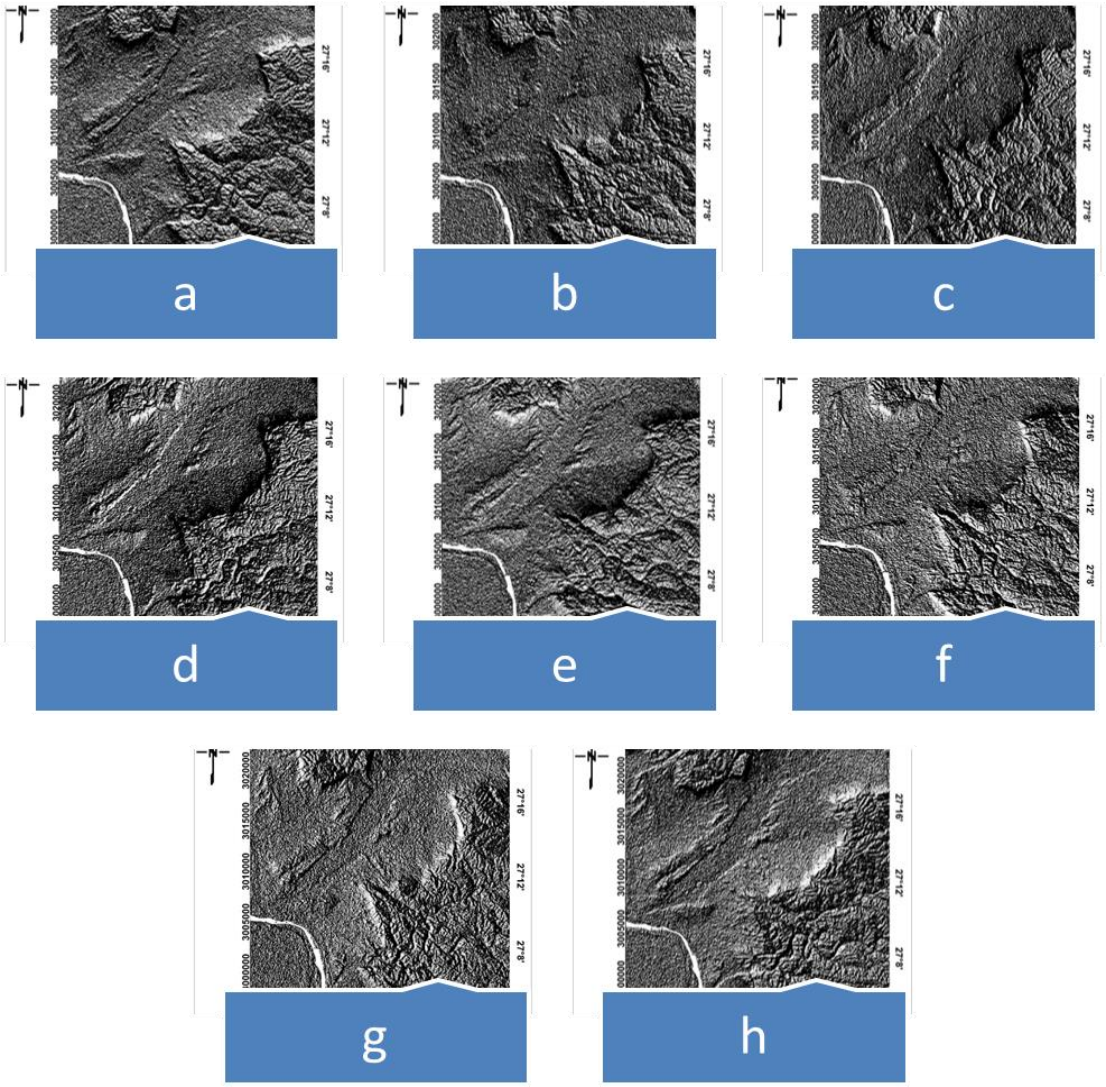

Fig. 6. Shaded relief images derived from DEM at sun angles: a) Sun angle: 0º, b) Sun angle: 45º, c) Sun angle: 90º, d) Sun angle: 135º, e) Sun angle: 180º, f) Sun angle: 225º, g) Sun angle: 270º and h) Sun angle: 315º.

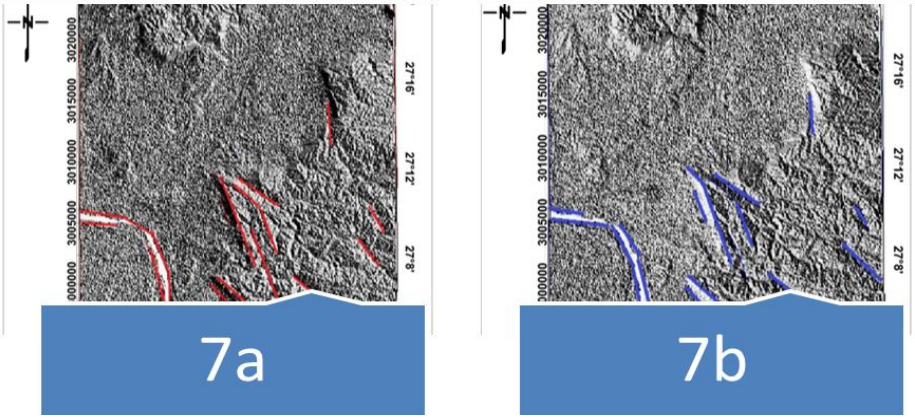

Fig. 7a. Shaded relief image created by combining four shaded relief images with sun angles of (0°, 45°, 90° and 135°) and lineaments extraction.

Fig. 7b. Shaded relief image created by combining four shaded relief images with sun angles of (180°, 225°, 270° and 315°) and lineaments extraction.

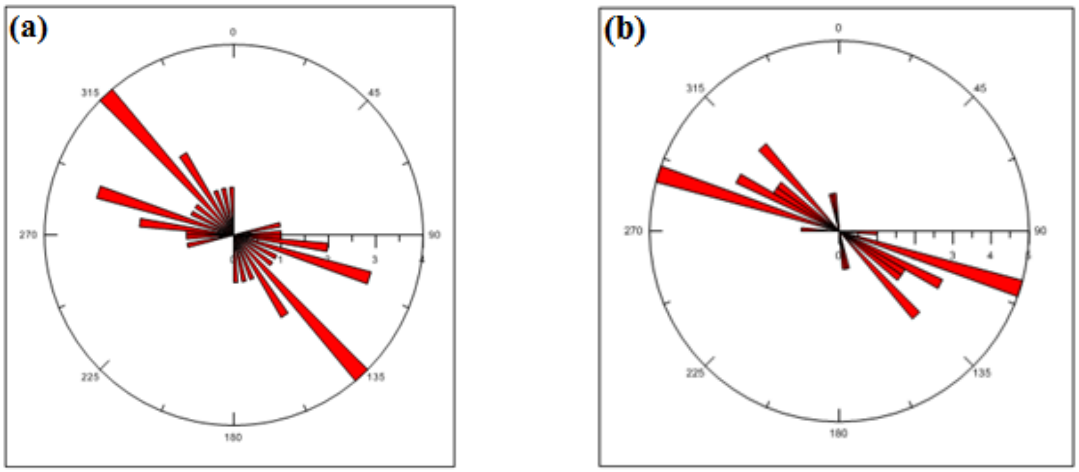

Figs. 8 a and b. Rose diagrams of; a: four shaded relief images with sun angles of (0°, 45°, 90° and 135°) and b: four shaded relief images with sun angles of (180°, 225°, 270° and 315°.

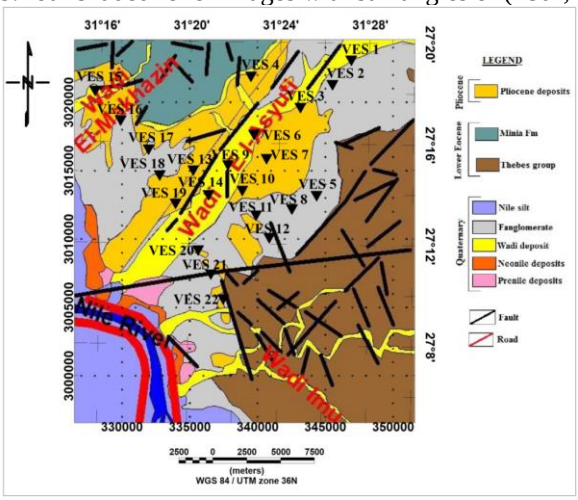

Fig. 9. Plotting of VES's locations at geologic map.

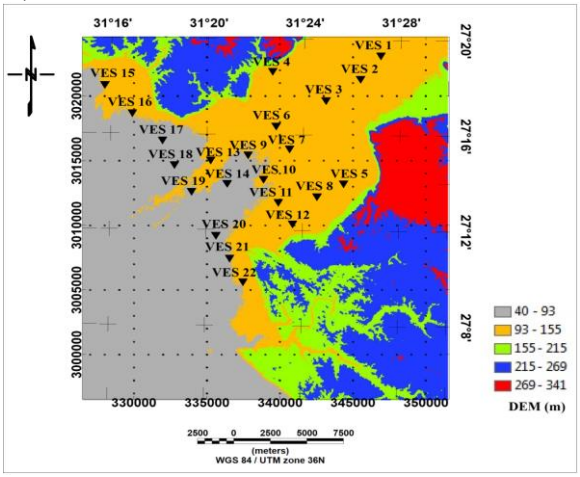

Fig. 10. Plotting of VES's locations at digital elevation model.

4.3. Geo-electric data analysis and drilling data

Zohdy and Resist geo-electric resistivity software's were displayed to interpret the measured geo-electric resistivity data in the study area [10, 11]. The data have been interpreted quantitatively by using the Ato program of [10] to obtain the initial multi-layer model, and Resist program of [11] to obtain the layering model. Figure 11 reflected an example of interpreted VES's by using Zohdy and Resist geo-electric resistivity software's and table 1 showed resistivity parameters of geo-electric layers from Resist layering program.

The first surficial resistive layer of wadi deposit with resistivity ranging of 347.4 to 9634.9 Ω.m with average thickness 1.53 m [12] the second geo-electric ranged between 11.2 to 1538.9 Ω.m with average thickness 8.26 m, the third layer ranged between 2.2 to 115.6 Ω.m with average thickness 29.77 m and the fourth layer ranged between 2.7 to 58.6 Ω.m with average thickness 81 m. Three constructive geo-electric cross sections (A-A\, B-B\ and C-C\) which illustrate the distribution of the different geo-electric layers in the study area (Figures 12, 13 & 14). It is mentioning that the first geo-electric layer (wadi sediments) is very thin and very high resistive layer, the second layer represented by fine sand, the third layer reflect clay intercalation with limestone and silt and the fourth layer represented by clay intercalation with sand and clay and refer to a good aquifer. The first geo-electric cross section A-A\ passes through VES's 15, 16, 17, 18, 19, 20, 21 and 22, the second geo-electric cross section B-B\ passes through VES's 3, 6, 9 and 14 and the third geo-electric cross section C-C\ passes through VES's 1, 2, 7, 10 and 20. Several normal faults have been recorded at these cross sections which forming horst and graben.

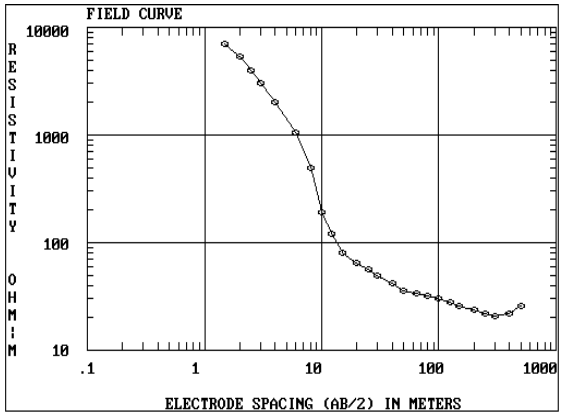

A) Field curve of VES (22) using Ato program [10]

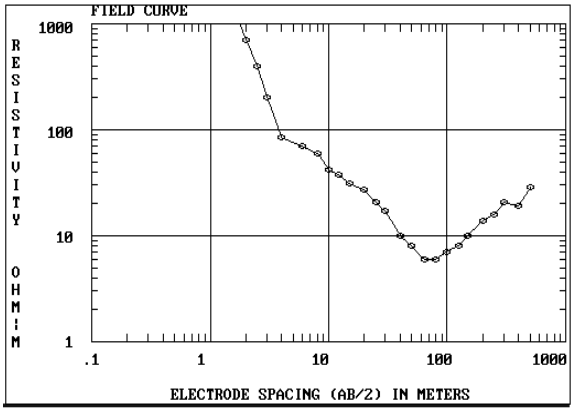

A) Field curve of VES (12) using Ato program [10]

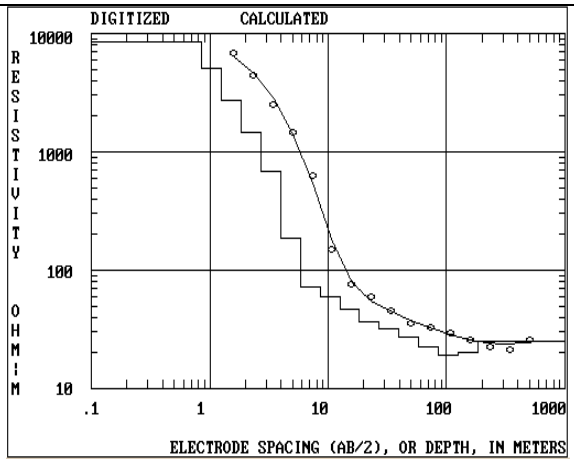

B) Geo-electric multi-layer modeling of VES (22) using Ato program [10]

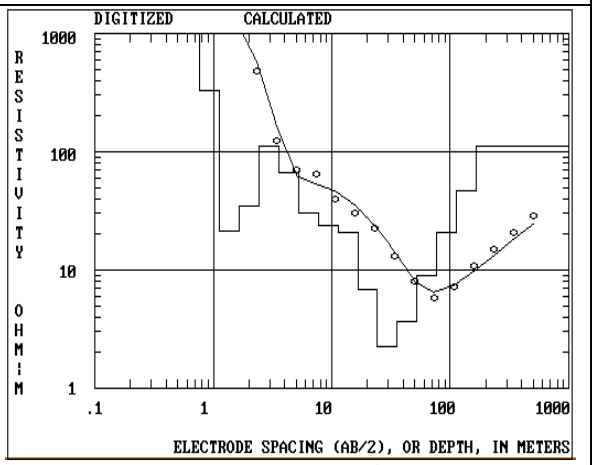

B) Geo-electric multi-layer modeling of VES (12) using Ato program [10]

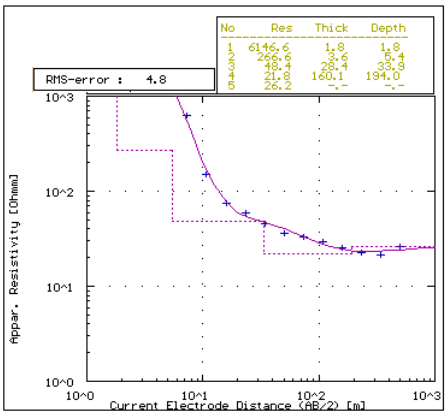

C) Geo-electric layer modeling of VES (22) using Resist [11]

(a)

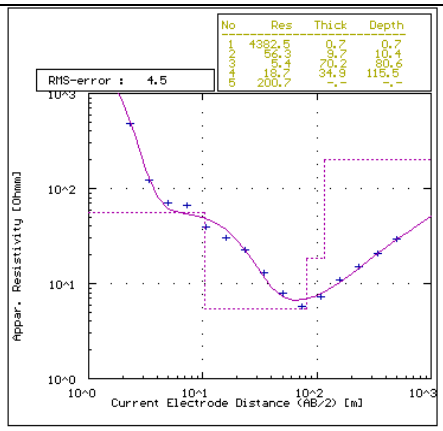

C) Geo-electric layer modeling of VES (12) using Resist [11]

(b)

VES#12

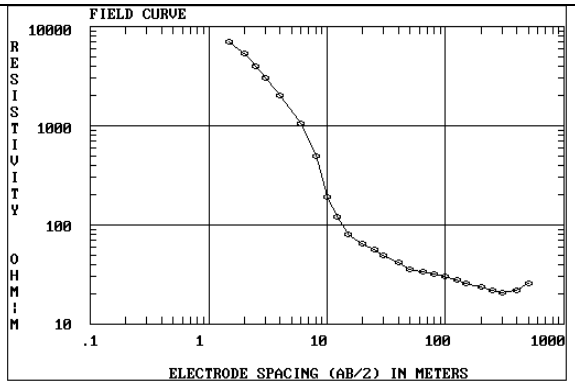

A) Field curve of VES (22) using Ato program [10]

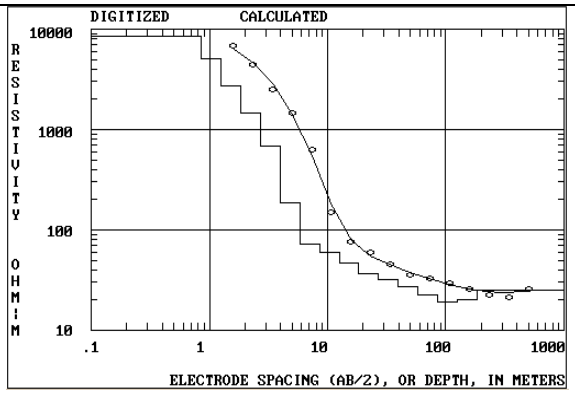

B) Geo-electric multi-layer modeling of VES (22) using Ato program [10]

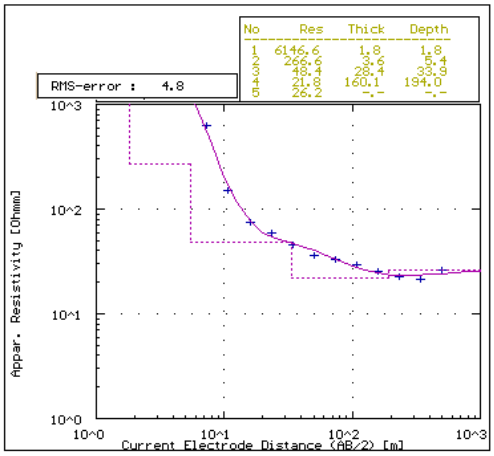

C) Geo-electric layer modeling of VES (22) using Resist [11]

(c)

VES#22

Fig. 11a,b & c. Examples of the interpreted VES's using Zohdy and Resist geo-electric resistivity software's.

Table (1): Resistivity parameters of geo-electric layers from Resist layering program [11].

VES No.	Parameters	Geo-electric Layers			
		1	2	3	4
VES 1	ρ (Ohm.m)	2266.4	103.8	23.1	39.2
	h (m)	1.4	7.8	55.3	113.1
	d (m)	1.4	9.2	64.5	177.6
VES 2	ρ (Ohm.m)	1442.1	56.8	8.9	40.8
	h (m)	2.5	12.5	46.6	31.6
	d (m)	2.5	15	61.6	93.2
VES 3	ρ (Ohm.m)	1763.5	106.4	34.6	10.4
	h (m)	2.8	2.8	22	120.4
	d (m)	2.8	5.6	27.6	148.0
VES 4	ρ (Ohm.m)	1475.9	678.8	26.7	5.8
	h (m)	3.6	11.4	7.7	44.7
	d (m)	3.6	15	22.7	67.4
VES 5	ρ (Ohm.m)	9634.9	582.1	76.2	2.7
	h (m)	0.7	3.3	15.3	48.3
	d (m)	0.7	4	19.4	67.7
VES 6	ρ (Ohm.m)	2601.2	11.2	2.2	58.6
	h (m)	0.9	7.5	21.1	31
	d (m)	0.9	8.3	29.4	60.4
VES 7	ρ (Ohm.m)	4720.5	180	18.1	5.6
	h (m)	1.8	9.8	18.6	69.6
	d (m)	1.8	11.7	30.3	99.9
VES 8	ρ (Ohm.m)	3232.1	69.5	2.3	10.6
	h (m)	1.9	12.4	28.9	28.4
	d (m)	1.9	14.3	43.1	71.5
VES 9	ρ (Ohm.m)	6554.9	641.5	9	31.3
	h (m)	0.8	11.7	24.3	70.4
	d (m)	0.8	12.5	36.7	107.2
VES 10	ρ (Ohm.m)	347.4	82.5	3.1	21.8
	h (m)	0.7	11.9	29.1	30.7
	d (m)	0.7	12.6	41.7	72.3
VES 11	ρ (Ohm.m)	367.2	12.4	2.5	13.1
	h (m)	2.7	14.6	37.9	36.3
	d (m)	2.7	17.3	55.2	91.4
VES 12	ρ (Ohm.m)	4382.5	56.3	5.4	18.7
	h (m)	0.7	9.7	70.2	34.9
	d (m)	0.7	10.4	80.6	115.5
VES 13	ρ (Ohm.m)	5167.2	194.5	75.9	9.3
	h (m)	0.9	4.3	60.8	122.3
	d (m)	0.9	5.2	66.1	188.3
VES 14	ρ (Ohm.m)	4321.4	318.7	44.5	9.6
	h (m)	0.8	2.6	14.8	162.9
	d (m)	0.8	3.4	18.2	181
VES 15	ρ (Ohm.m)	1232	323.9	14.6	21.3
	h (m)	2	11.1	30.5	72.3
	d (m)	2	13.3	43.6	115.9
VES 16	ρ (Ohm.m)	7383.8	517.6	65.1	8.7
	h (m)	0.9	2.5	21.9	55.4
	d (m)	0.9	3.4	25.3	80.7
VES 17	ρ (Ohm.m)	3817.6	96.2	12.3	6.9
	h (m)	2.1	12.1	16.8	71.2
	d (m)	2.1	14.2	31	102.1
VES 18	ρ (Ohm.m)	7110.1	474.4	115.6	10
	h (m)	2.2	14.7	10	174.7
	d (m)	2.2	16.9	26.8	201.5
VES 19	ρ (Ohm.m)	9120.7	1538.9	31.4	11.5
	h (m)	0.8	2.3	44.9	94.8
	d (m)	0.8	3.1	48	142.8
VES 20	ρ (Ohm.m)	1269.7	112.8	52.6	6
	h (m)	0.9	6.6	24.4	62
	d (m)	0.9	7.5	31.9	93.9
VES 21	ρ (Ohm.m)	3691.8	277.2	37.3	18.6
	h (m)	1.3	6	44.7	137
	d (m)	1.3	7.3	52.1	189.1
VES 22	ρ (Ohm.m)	6146.6	266.6	48.4	21.8
	h (m)	1.8	3.6	28.4	160.1
	d (m)	1.8	5.4	33.9	194

Explanation: ρ is the true resistivity value, h is the thickness of layer and d is the depth of layer

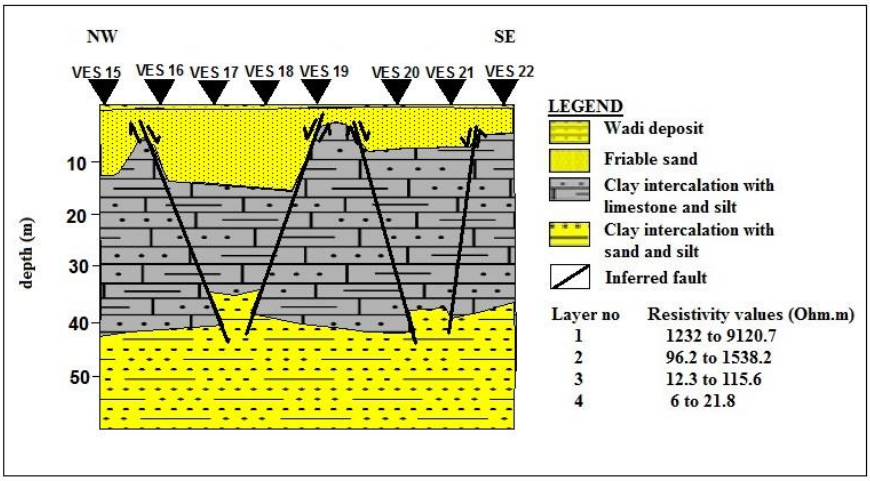

Fig. 12. 2D geo-electric cross section A-A\ passes through VES's 15, 16, 17, 18, 19, 20, 21 and 22

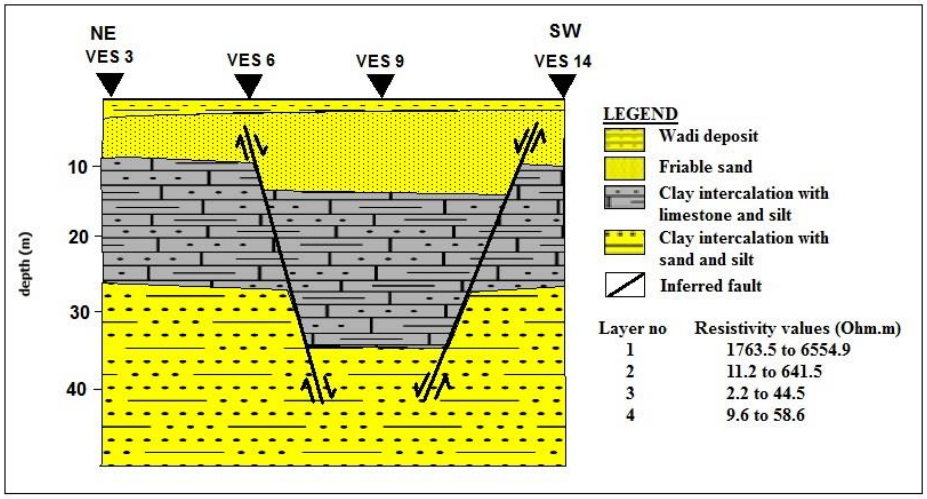

Fig. 13. 2D geo-electric cross section B-B\ passes through VES's 3, 6, 9 and 14.

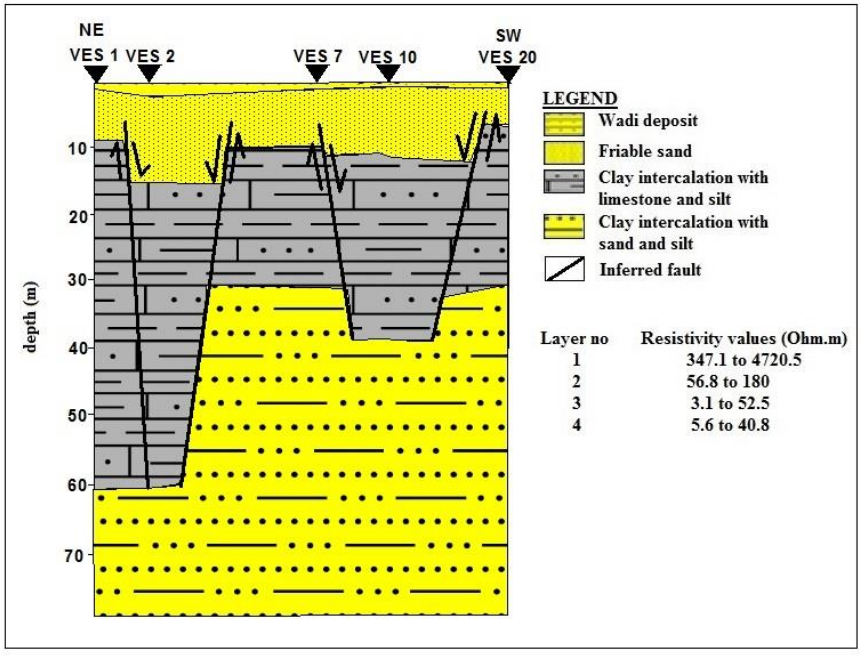

Fig. 14. 2D geo-electric cross section C-C\ passes through VES's 1, 2, 7, 10 and 20.

Figure 15 summarizes the correlation between VES 22 and WELL 1 and gives brief description about subsurface succession as follows; Unit no.1) It represented the surface layer Wadi deposit, friable sand, fine sand, clay and limestone and characterized by high resistivity value, Unit no.2) composed of clay intercalation with limestone and silt and Unit no.3) The aquifer layer, which characterized by low resistivity value and composed of clay intercalation with sand and silt.

4.4. Distribution of aquifer layer

The results showed that, the aquifer layer is represented by the Pre-Nile deposits and belongs the Pleistocene age, which composed of sandy clay. Figure 16 showed the thickness distribution map of aquifer layer, the largest thickness (suitable locations for drilling) located at the northeast, northwest, west, southwest and the southern parts of the area, which included VES's 1, 3, 13, 14, 15, 18, 19, 20, 21 and 22. According to geo-electric value the average thickness of this layer approximately 81 m and the resistivity value ranged between 2.7 to 58.6 Ω. The high resistivity zones are interpreted as relatively high quality of the groundwater and low of salinity content and vice versa.

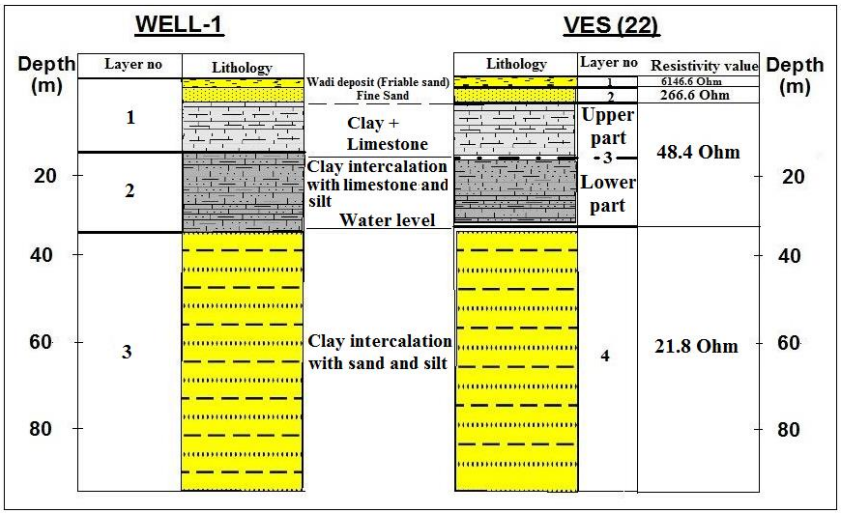

Fig. 15. Correlation between results of WELL-1 and VES 22.

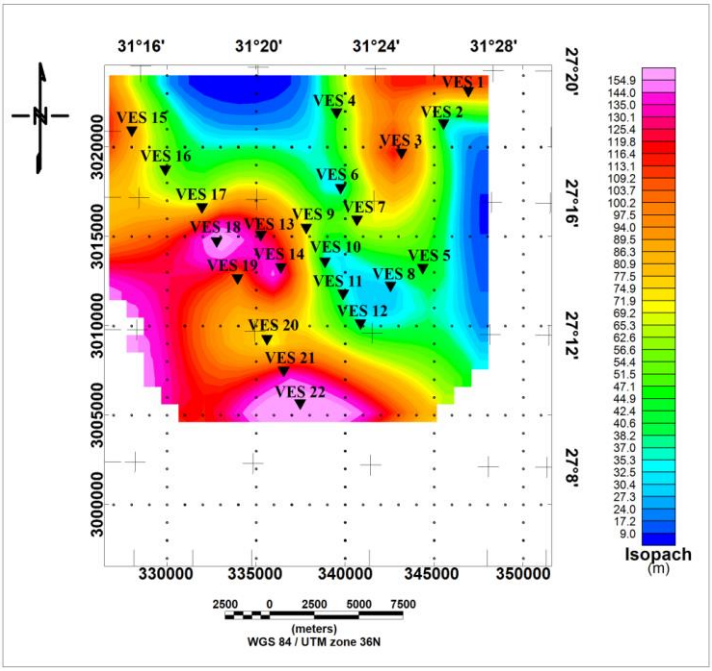

Fig. 16. Thickness distribution map of the forth layer (aquifer layer).

5. CONCLUSIONS

The extracted surface lineaments which derived from geology and remote sensing reflected five main trends; NW-SE, WNW-ESE, NE-SW, N-S and E-W directions.

Subsurface stratigraphic succession of the study area consists of; Wadi deposit, friable sand, fine sand, clay and limestone which represented the first layer, the second layer composed of clay intercalation with limestone and silt and the aquifer layer characterized by low resistivity value and composed of clay intercalation with sand and silt. The water bearing layer increase at the northeast, northwest, west, southwest and the southern parts of the area and the and decreases at the east and north parts of the area (fig 16).

REFERENCES

[1] Bakheit, A A. Geological and geophysical studies on the areas around Wadi El-Assiuti, Eastern Desert, Egypt. Ph.D. Thesis, Geol. Dept., Assiut Univ.1989; 203. p.

[2] Ashmawy, M H and Nassim, A S. Hydrogeologic impact and assessement of morphometric aspects of wadi el Asyuity basin, Eastern desert, Egypt.Tanta University. Egyptian journal of remote sensing and space science.1998; vol.1, no.1: pp.207-232.

[3] Mohamaden, M I.Geoelectrical Survey for Groundwater Exploration at the Asyuit Governorate, Nile Valley, Egypt. Marine Scienes.2009; 20 (1).

[4] Abotalib, A Z and Mohamed, R S. Surface evidences supporting a probable new concept for the river systems evolution in Egypt. A remote sensing overview. 2013; 69(5): pp.1621-1635.

[5] El Tahlawi, M R, Abo-El Kassem, M, Baghdadi, G Y and Saleem, H A. Assessment of groundwater Vulnerability a case study. International Journal of Advanced Remote Sensing and GIS.2016; pp-1561.

[6] Refaat, m. Integrated Interpretaion of land Geophysical surveys and Remote Sensing data for groundwater horizons detection at new assiut city- el safa city, western desert Egypt. M.Sc. Thesis, Geol. Dept., al-azhar Univ.2018.

[7] Conoco. Geological Map of Egypt, Scale 1: 500,000, -NG 36NW- Asyut, Egypt. The Egyptian General Petroleum Corporation, Cairo (EGPC), Egypt.1987.

[8] Abdallah, M S. the Najd Fault System. King Fahd University of Petroleum & Minerals. 2016; https://www.researchgate.net/ation/3public1388 1827_The_Najd_Fault_System.

[9] http://earthexplorer.usgs.gov. USGS: Science for a changing world. U.S. Department of the Interior U.S. Geological Survey- Page Contact Information:custserv@usgs.gov.

[10] Zohdy, A A R and Bisdorf, R J. Programs for the automatic processing and interpretation of Schlumberger sounding curves in Quick Basic; U.S. Geological Survey Open File Report .1989; 89-137-2, 64 p.

[11] Velpen, B P A. Resist program, M.Sc. Research project, ITC, Holland.1988;v.1.0.

[12] Sadek, H S, Soliman, S A and Abdulhadi, H M. A correlation between the different models of resistivity sounding data to discover new fresh water fields in El Sadat City, Western Desert of Egypt. Proc. of the 7PUthUP International Mathematical Geophysics Seminar, Free University of Berlin. 1987; 329-346.

تحديد التراكيب السطحية واستكشاف المياه الجوفية باستخدام نظم المعلومات الجغرافية والنتائج الجيوكهربية بمنطقة وادي الاسيوطي – الصحراء الشرقية – مصر.

أشرف محمد عبده [1] ، حسن صالح ثابت [2] ، محمد السعيد معبد [2]

[1] قسم الجيولوجيا, كلية العلوم, جامعة الازهر,القاهرة, مصر.
[2] الهيئة المصرية العامة للثروة المعدنية,القاهرة,مصر

الملخص:

تقع منطقة الدراسة بمدينة أسيوط الجديدة - الصحراء الشرقية – مصر ما بين خطى طول ″00 ′15 °31 و ″00 ′30 °31 شرقا و خطى عرض ″00 ′05 °27 و ″00 ′20 °27 شمالا بمساحة قدرها 675,1 كم^2 . ويهدف البحث الي : دراسة التراكيب السطحية بالاضافة الي التعرف علي التتابع الطبقي التحت سطحي و إستكشاف مكامن المياه الجوفية بمنطقة الدراسة. وقد تم استخدام بيانات الاستشعار عن بعد ومعالجتها بنظم المعلومات الجغرافية بالاضافة الي استخدام الجسات الجيوكهربية (تقنية شلمبرجير). وقد تم استخدام نموذج الارتفاع الرقمي المشتق من صور الاقمار الصناعية حيث اظهر بشكل واضح طبوغرافية المنطقة ومن ثم تم اشتقاق خرائط الظل من هذا النموذج والتي بدورها قامت بإخراج التراكيب السطحية للمنطقة. وقد اوضحت الجيولوجيا وصور الاقمار الصناعية التراكيب السطحية لمنطقة الدراسة والتي تاخذ اتجاهات (شمال شرق/ جنوب غرب) – (شمال غرب / جنوب شرق) – (شمال- جنوب / شرق-غرب).اما عن الجسات الجيوكهربية فقد بينت التتابع التحت سطحي للمنطقة واكدتها نتائج الحفر ويشمل التتابع التحت سطحي لمنطقى الدراسة ما يلي: طبقة الرواسب الوديانية – طبقة الرمال الناعمة – طبقة خليط من الطفلة والحجر الجيرى والطين – طبقة خليط من الطفلة والرمال والطين وهي طبقة الخزان الجوفي لمنطقة الدراسة.

تحتوي الدراسات الرسوبية دراسة التحليل الحجمي للحبيبات ودراسة التركيب المعدني والدراسة البتروجرافية وذلك لتحديد القياسات الإحصائية ومعاملات التدرج الحبيبي اللازمة لوصف أنماط الترسيب للعينات الرسوبية بمنطقة الدراسة ، وتشتمل هذه المعاملات الإحصائية علي متوسط حجمي بمتوسط 1.205ϕ وهذا يشير أن الرمال ذات حجم متوسط الحبيبات، وفرز الحبيبات بمتوسط 2.297ϕ وهذا يعني أن الحبيبات فقيرة الفرز جدا ومعامل الالتواء بمتوسط 0.361ϕ مما يعني أن الحبيبات عالية الالتواء جدا ومعامل التفرطح بمتوسط 1.26ϕ مما يدل أن الحبيبات مدببة التفرطح وعند عمل العلاقات بين معاملات التحليل الحجمي المختلفة تبين أن بيئة الترسيب السائدة في منطقة الدراسة هي بيئة نهرية . وتبين من تحليل الحيود للأشعة السينية للعينات المدروسة أن المعادن الطينية هي المنتموريلونايت والكاولينيت. وقد أبدت الدراسة البتروجرافية التي أجريت علي 8 عينات وجود التربة الفتاتية متمثلة في الحجر الرملي و الطيني وتبين منها أن المادة اللاحمة في التربة الفتاتية هي السيليكا والكربونات ووجود بقايا من البازلت المتحلل وتبين منها وجود بعض التغيرات.

وأظهرت الدراسة الإشعاعية نشاطية النويات المشعة للثوريوم واليورانيوم والبوتاسيوم و مكافئ الراديوم بمتوسطات 7.09 و15.41 و249.12 و80.78 بيكريل/كجم على الترتيب بينما متوسطات معدل الجرعة الفعالة(D_{eff}) ومؤشر الخطر الخارجي(H_{ex}) يمثل 38.15 ميكروسيفر/سنة و0.218 بيكريل/كجم علي الترتيب وتعد هذه القيم أقل بكثير من القيم المسموح بها من قبل الوكالة الدولية للطاقة الذرية للأمان الإشعاعي ومن النتائج السابقة تبين أن منطقة الدراسة آمنة اشعاعيا.